

Title: DNGR-1 in DCs limits tissue damage by dampening neutrophil recruitment

Authors: Carlos del Fresno^{1, ‡, *}, Paula Saz-Leal^{1, ‡}, Michel Enamorado¹, Stefanie K. Wculek¹, Sarai Martínez-Cano¹, Noelia Blanco-Menéndez¹, Oliver Schulz², Mattia Gallizioli³, Francesc Miró³, Eva Cano⁴, Anna Planas^{3,5}, David Sancho^{1,*}

Affiliations:

¹ Immunobiology Laboratory. Centro Nacional de Investigaciones Cardiovasculares (CNIC), Madrid, Spain

² Immunobiology Laboratory, The Francis Crick Institute, London, UK

³ Institut d'Investigacions Biomèdiques August Pi i Sunyer (IDIBAPS), Barcelona, Spain

⁴ Chronic Disease Programme-CROSADIS, Instituto De Salud Carlos III, Madrid, Spain

⁵ Department of Brain Ischemia and Neurodegeneration, Institut d'Investigacions Biomèdiques de Barcelona (IIBB-CSIC), Barcelona, Spain

M.E. current address: Mucosal Immunology Section, Laboratory of Parasitic Diseases, NIAID, NIH, Bethesda, MD 20892, USA

*Correspondence to:

David Sancho

Carlos del Fresno

Centro Nacional de Investigaciones Cardiovasculares Carlos III (CNIC)

Melchor Fernández Almagro, 3

E-28029, Madrid, Spain

Tel: (+ 34) 914531200 Ext 2010

Tel (direct line): (+ 34) 662 990 4777 2010

FAX: (+ 34) 914531245

E-mail:

dsancho@cnic.es

cdelfresno@cnic.es

‡ Co-first authors

Abstract:

Host injury triggers feedback mechanisms that limit tissue damage. Classical type-1 dendritic cells (cDC1s) express DNGR-1/*CLEC9A*, which senses tissue damage and favors cross-presentation of dead-cell material to CD8⁺ T cells. Here, we find that DNGR-1 additionally reduces host-damaging inflammatory responses induced by sterile and infectious tissue injury. DNGR-1-deficiency leads to exacerbated caerulein-induced necrotizing pancreatitis and increased pathology during systemic *Candida albicans* infection without impacting fungal burden. This effect is B- and T-cell-independent and attributable to increased neutrophilia in DNGR-1-deficient settings. Mechanistically, DNGR-1 engagement activates SHP-1 and inhibits Mip-2/Cxcl2 production by cDC1s during *Candida* infection. This consequently restrains neutrophil recruitment and promotes disease tolerance. Thus, DNGR-1-mediated sensing of injury by cDC1s serves as a rheostat for the control of tissue damage, innate immunity, and immunopathology.

One Sentence Summary:

DNGR-1-mediated sensing of injury by cDC1s reduces immunopathology by attenuating neutrophil infiltration of damaged tissues.

Main Text:

Following sterile or infectious insults, injured tissues expose alarm signals that are detected by specific innate immune receptors on myeloid cells (1). This triggers an inflammatory response, which promotes the recruitment of myeloid cells into the damaged organ. This innate immune response must be tightly regulated to avoid additional tissue damage (2).

Among myeloid cell sensors of tissue damage, DNGR-1 (*Clec9a* gene) is a C-type lectin receptor (CLR) that detects F-actin exposed by damaged cells (3, 4). DNGR-1 is mainly expressed by mouse and human classical type 1 dendritic cell (cDC1), including CD103⁺CD11b⁻ DCs in peripheral tissues (5, 6). DNGR-1 favors the cross-presentation of dead cell-associated antigens to CD8⁺ T cells (7-9). However, whether DNGR-1 plays any role in innate immunity is unknown. To address this issue, we used a mouse model of caerulein-induced acute necrotizing pancreatitis (Fig. 1A), which results in massive acinar cell death, leading to the infiltration of myeloid cells. This, in turn, triggers further pathology and edema (10). Upon caerulein treatment, there was increased pancreatic infiltration by neutrophils but not monocytes in DNGR-1-deficient (*Clec9a*^{gfp/gfp}) compared to wild-type (WT) mice (Fig. 1B). Neutrophil numbers in the bone marrow (BM) and blood were comparable in both genotypes (fig. S1), ruling out an effect of DNGR-1 deficiency on neutrophil ontogeny and suggesting a local recruitment effect.

As a non-genetic approach, we used an anti-DNGR-1-blocking antibody (7, 11). Receptor blockade phenocopied the exacerbated pancreatic infiltration of neutrophils (Fig. 1C) but not monocytes (fig. S2A). Enhanced neutrophilia upon DNGR-1-blockade was lost in *Batf3*^{-/-} mice (Fig. 1D and fig. S2B), which lack functional cDC1s (12), indicating that cDC1s are the key mediators. Pancreatic CXCR2-mediated neutrophil infiltration is pathological in acute

pancreatitis (13). Consistently, caerulein-treated *Clec9a^{gfp/gfp}* mice displayed exacerbated pancreatitis with raised serum lipase (Fig. 1E) and extended pancreatic edema (Fig. 1F).

The rapid kinetics of neutrophil infiltration suggested the involvement of an innate immune response. To test this, *Rag1^{-/-}* (lacking B and T cells) and *Rag1^{-/-}Clec9a^{gfp/gfp}* mice were subjected to caerulein-induced acute pancreatitis. Notably, the absence of DNGR-1 resulted in enhanced neutrophil infiltration (Fig. 1G and fig. S2C) and elevated circulating lipase levels (Fig. 1H) in B- and T-cell-deficient mice. Thus, following tissue damage, DNGR-1 expressed on cDC1s regulates the recruitment of neutrophils without the involvement of B and T cells.

A reduction of neutrophil-mediated immunopathology is associated with disease tolerance upon infection, which limits the impact of damage-generating infectious challenges on host fitness without affecting pathogen burden (14, 15). To test whether DNGR-1 affects disease tolerance, we used systemic *Candida albicans* infection, which generates extensive renal tissue necrosis (16). DNGR-1-deficient mice showed increased morbidity and mortality upon systemic candidiasis (Fig. 2A, B), despite having a similar fungal burden (Fig. 2C). Extended pathology in the absence of DNGR-1 correlated with increased neutrophil infiltration in the kidney (Fig. 2D, E). Neutrophil numbers in BM or blood of WT and *Clec9a^{gfp/gfp}* mice were similar (fig. S3). DNGR-1 blockade in infected mice phenocopied increased neutrophilia (Fig. 2F), which was prevented in *Batf3*-deficient mice (Fig. 2G), indicating that cDC1s mediate the effect. Of note, *Rag1^{-/-}Clec9a^{gfp/gfp}* mice also showed elevated renal neutrophil numbers (Fig. 2H), and reduced survival after infection (Fig. 2I). Monocyte recruitment into *Candida*-infected kidneys was not significantly increased in any of the DNGR-1-deficient conditions (Fig. 2D, right and fig. S4). Thus, DNGR-1 dampens the recruitment of neutrophils to damaged tissues both in sterile and infectious settings in a B- and T-cell-independent manner.

Neutrophil-mediated renal immunopathology causes acute kidney failure and mortality during systemic candidiasis (17, 18). Consistently, *C. albicans*-infected *Clec9a^{gfp/gfp}* mice showed exacerbated kidney damage, with increased TUNEL-positive cells (Fig. 2J), elevated levels of serum creatinine (Fig. 2K), and enhanced expression of kidney injury molecule-1 (Kim-1) (Fig. 2L). Kidney neutrophilia was increased in *Clec9a^{gfp/gfp}* mice three days after infection (Fig. 2M), along with enhanced Kim-1 expression (Fig. 2N). Thus, exacerbated renal damage caused by neutrophils could underlie increased pathology *Candida*-infected *Clec9a^{gfp/gfp}* mice.

We tested whether DNGR-1-regulated neutrophilia drives tissue damage in sterile pancreatitis (Fig. 3A). Partial depletion of neutrophils using anti-Ly6G 1A8 antibody (fig. S5) reverted the enhanced edematous lesions found in isotype-treated *Clec9a^{gfp/gfp}* mice upon caerulein-treatment (Fig. 3B). Assessing the impact of neutrophils in *C. albicans* infection is more complex, as the depletion of neutrophils is lethal (19). To circumvent this, we first used fungizone to eliminate the fungus starting at day 3 post-infection (Fig. 3C and fig. S6A), after initial tissue damage by the infection (Fig. 2N). Removal of *C. albicans* did not affect the exacerbated neutrophil infiltration (Fig. 3D) or renal damage (Fig. 3E) observed in *Clec9a^{gfp/gfp}* mice. Thus, after the initial damage, the presence of fungus was not essential for the DNGR-1-dependent effect. Neutrophil depletion with anti-Ly6G (1A8) in the presence of fungizone (Fig. 3C, F and fig. S6B) prevented the enhanced renal damage found in isotype-treated *Clec9a^{gfp/gfp}* mice (Fig. 3G, H), despite fungal burden was equivalent between genotypes (Fig. 3I). Thus, neutrophil influx is the cellular mechanism driving the pathology in *Candida*-infected *Clec9a^{gfp/gfp}* mice.

To decipher the mechanisms underlying the regulatory role of DNGR-1 on cDC1s in neutrophil infiltration, we used F-actin/myosin II complexes (DNGR-1L) to robustly trigger the

receptor (20). Plated DNGR-1L triggered signaling through the DNGR-1/Syk axis in B3Z-NFAT reporter cells (7) in a dose- (fig. S7A) and DNGR-1-dependent manner (fig. S7B). Then, we used a cDC1 cell line (MutuDC) (21) that expresses DNGR-1 as well as Dectin-1 (fig. S8A), a CLR critically involved in *C. albicans* recognition (22). Stimulation of MutuDCs with the Dectin-1 agonists whole beta-glucan particles (WGP) or heat-killed *Candida albicans* (HKC) (23) induced the expression of proinflammatory factors such as *Tnf*, *Mip-2/Cxcl2*, and *Egr2*. This was reduced by concomitant exposure to DNGR-1L (Fig. 4A and fig. S8B, C). Consistently, DNGR-1 triggering attenuated PLC γ 2 phosphorylation and I κ B degradation in response to WGP (Fig. 4B). DNGR-1 triggering had no impact on the response to TLR9 ligand CpG (Fig. 4C and fig. S8D, E), indicating specificity in the pathways modulated. Using a blocking antibody (fig. S8F), we confirmed that the effect elicited by DNGR-1L was DNGR-1 dependent (fig. S8G).

Regulatory phosphatases can couple to some ITAM-containing receptors (24, 25). As DNGR-1 bears a hemITAM motif (7), we tested phosphatase activation upon DNGR-1L sensing. DNGR-1L induced SHP-1 phosphorylation (Fig. 4D) without impacting other CLR-related regulatory mechanisms (26, 27) (fig. S8H). Treatment with the SHP inhibitor NSC-87877 (NSC) abolished the regulatory effect of DNGR-1L on responses elicited by WGP (Fig. 4E). Moreover, mice with SHP-1 depletion in the CD11c⁺ compartment (CD11c Δ SHP-1) (28), including cDC1s, phenocopied the exacerbated neutrophil infiltration observed in DNGR-1-deficient mice (Fig 4F and fig. S9). These observations are consistent with an involvement of SHP-1 in the molecular mechanism that adjusts inflammatory responses in cDC1s following DNGR-1 engagement.

Mip-2/Cxcl2 is a CXCR2 ligand fundamental for neutrophil mobilization from the bone marrow (29) and local recruitment to *C. albicans*-infected tissues (30). We hypothesized that the *Mip-2/CXCR2* axis could be mediating the boosted neutrophilia in the absence of DNGR-1.

Administration of pepducin, a peptide that inhibits CXCR2 signaling (13), reverted the enhanced renal neutrophil recruitment observed in *Clec9a^{gfp/gfp}* upon *Candida*-infection (Fig. 4G). In order to dissect the contribution of DNGR-1 to the Mip-2-mediated process in vivo, we infected mice with *C. albicans*. Sixty hours later, we measured *Cxcl2* expression in the renal immune infiltrate (fig. S10). Of all ten immune populations tested, only neutrophil frequencies were increased in *Clec9a^{gfp/gfp}* mice (fig. S11). *Cxcl2* was expressed by neutrophils, macrophages, cDC2s, and cDC1s, but expression was enhanced only in cDC1s in *Clec9a^{gfp/gfp}* mice (Fig. 4H). This suggests that DNGR-1 limits *Cxcl2* expression in cDC1s during *C. albicans* infection.

To investigate the relevance of this increased Mip-2 production by cDC1s on neutrophil recruitment under DNGR-1-deficient settings, we generated mixed BM chimeric mice with specific Mip-2 deficiency in cDC1s (*Batf3^{-/-}:Cxcl2^{-/-}*) (see Methods and fig. S12). Following infection with *C. albicans*, DNGR-1 blockade generated an exacerbated renal neutrophil recruitment in *Batf3^{-/-}:WT* control chimeras (Fig. 4I). This boosted neutrophilia was lost in *Batf3^{-/-}:Cxcl2^{-/-}* chimeras (Fig. 4I), thus relying on *Cxcl2*/Mip-2 produced by cDC1s.

Furthermore, we crossed *Clec9a^{gfp/gfp}* and *Cxcl2^{-/-}* mice to further generate chimeric mice with cDC1s lacking both DNGR-1 and Mip-2 (*Batf3^{-/-}:Clec9a^{gfp/gfp} Cxcl2^{-/-}*). Upon systemic candidiasis, *Batf3^{-/-}:Clec9a^{gfp/gfp}* chimeras showed an exacerbated neutrophil infiltration into the kidney compared with *Batf3^{-/-}:WT* control chimeras (Fig. 4J). Notably, this boosted neutrophilia was lost in *Batf3^{-/-}:Clec9a^{gfp/gfp} Cxcl2^{-/-}* mice (Fig. 4J). Thus, in the absence of DNGR-1, Mip-2 produced by *Batf3*-dependent cDC1s is a key mediator for the enhanced neutrophil recruitment.

Infiltration of immune cells within injured tissues must balance pathogen control with increased damage caused by the inflammatory response. In particular, early infiltration by neutrophils to damaged tissues must be carefully regulated, as these cells can cause further tissue

destruction (13, 17, 18). Disease tolerance to infections comprises mechanisms involved in the control of tissue damage. This concept of “tissue damage control” is not restricted to infections and can be also applied to the regulation of damage from sterile inflammation (14, 31). Notably, mediators involved in tissue damage control under both sterile and infectious conditions can be shared (31). Our data suggest that DNGR-1 acts as a shared checkpoint for sterile and infectious tissue damage control. Detection of tissue damage by cDC1s through DNGR-1 would act as a checkpoint for neutrophil infiltration and further immunopathology. Deficient sensing of tissue damage in the absence of DNGR-1 leads to higher production of Mip-2 by cDC1s. This increased Mip-2 production can ignite neutrophil infiltration that drives immunopathology within the damaged organ (fig. S13). Thus, DNGR-1 acts as a necrosis-sensing receptor that, depending on the inflammatory context, may promote a regulatory tissue damage control mechanism by cDC1s or may contribute to cross-priming during adaptive immunity related-responses (7-9). This capacity to develop two different host protective functions and the regulation and implications of this dual role remain to be investigated.

References and Notes:

1. P. Matzinger, The danger model: a renewed sense of self. *Science (New York, N.Y.)* 296, 301-305 (2002).
2. K. L. Rock, H. Kono, The inflammatory response to cell death. *Annu Rev Pathol* 3, 99-126 (2008).
3. S. Ahrens *et al.*, F-actin is an evolutionarily conserved damage-associated molecular pattern recognized by DNCR-1, a receptor for dead cells. *Immunity* 36, 635-645 (2012).
4. J.-G. Zhang *et al.*, The Dendritic Cell Receptor Clec9A Binds Damaged Cells via Exposed Actin Filaments. *Immunity* 36, 646-657 (2012).
5. B. U. Schraml *et al.*, Genetic Tracing via DNCR-1 Expression History Defines Dendritic Cells as a Hematopoietic Lineage. *Cell* 154, 843-858 (2013).
6. L. F. Poulin *et al.*, DNCR-1 is a specific and universal marker of mouse and human Batf3-dependent dendritic cells in lymphoid and nonlymphoid tissues. *Blood* 119, 6052-6062 (2012).
7. D. Sancho *et al.*, Identification of a dendritic cell receptor that couples sensing of necrosis to immunity. *Nature* 458, 899-903 (2009).
8. S. Iborra *et al.*, The DC receptor DNCR-1 mediates cross-priming of CTLs during vaccinia virus infection in mice. *J Clin Invest* 122, 1628-1643 (2012).
9. S. Zelenay *et al.*, The dendritic cell receptor DNCR-1 controls endocytic handling of necrotic cell antigens to favor cross-priming of CTLs in virus-infected mice. *J Clin Invest* 122, 1615-1627 (2012).

10. M. M. Lerch, F. S. Gorelick, Models of acute and chronic pancreatitis. *Gastroenterology* 144, 1180-1193 (2013).
11. S. Iborra *et al.*, Optimal Generation of Tissue-Resident but Not Circulating Memory T Cells during Viral Infection Requires Crosspriming by DNNGR-1+ Dendritic Cells. *Immunity* 45, 847-860 (2016).
12. K. Hildner *et al.*, Batf3 deficiency reveals a critical role for CD8alpha+ dendritic cells in cytotoxic T cell immunity. *Science (New York, N.Y.)* 322, 1097-1100 (2008).
13. C. W. Steele *et al.*, CXCR2 inhibition suppresses acute and chronic pancreatic inflammation. *J Pathol* 237, 85-97 (2015).
14. R. Medzhitov, D. S. Schneider, M. P. Soares, Disease tolerance as a defense strategy. *Science (New York, N.Y.)* 335, 936-941 (2012).
15. A. M. Jamieson *et al.*, Role of tissue protection in lethal respiratory viral-bacterial coinfection. *Science (New York, N.Y.)* 340, 1230-1234 (2013).
16. J. F. Fisher, K. Kavanagh, J. D. Sobel, C. A. Kauffman, C. A. Newman, Candida urinary tract infection: pathogenesis. *Clin Infect Dis* 52 Suppl 6, S437-451 (2011).
17. O. Majer *et al.*, Type I interferons promote fatal immunopathology by regulating inflammatory monocytes and neutrophils during Candida infections. *PLoS Pathog* 8, e1002811 (2012).
18. M. S. Lionakis *et al.*, Chemokine receptor Ccr1 drives neutrophil-mediated kidney immunopathology and mortality in invasive candidiasis. *PLoS Pathog* 8, e1002865 (2012).

19. T. Dejima *et al.*, Protective role of naturally occurring interleukin-17A-producing gammadelta T cells in the lung at the early stage of systemic candidiasis in mice. *Infection and immunity* 79, 4503-4510 (2011).
20. O. Schulz *et al.*, Myosin II Synergizes with F-Actin to Promote DNGR-1-Dependent Cross-Presentation of Dead Cell-Associated Antigens. *Cell Rep* 24, 419-428 (2018).
21. S. A. Fuertes Marraco *et al.*, Novel murine dendritic cell lines: a powerful auxiliary tool for dendritic cell research. *Front Immunol* 3, 331 (2012).
22. R. A. Drummond, G. D. Brown, The role of Dectin-1 in the host defence against fungal infections. *Curr Opin Microbiol* 14, 392-399 (2011).
23. H. S. Goodridge *et al.*, Activation of the innate immune receptor Dectin-1 upon formation of a 'phagocytic synapse'. *Nature* 472, 471-475 (2011).
24. S. Ben Mkaddem *et al.*, Shifting FcγRIIA-ITAM from activation to inhibitory configuration ameliorates arthritis. *J Clin Invest* 124, 3945-3959 (2014).
25. S. Iborra *et al.*, Leishmania Uses Mincle to Target an Inhibitory ITAM Signaling Pathway in Dendritic Cells that Dampens Adaptive Immunity to Infection. *Immunity* 45, 788-801 (2016).
26. N. Blanco-Menendez *et al.*, SHIP-1 Couples to the Dectin-1 hemITAM and Selectively Modulates Reactive Oxygen Species Production in Dendritic Cells in Response to *Candida albicans*. *J Immunol* 195, 4466-4478 (2015).
27. T. S. Freedman *et al.*, LynA regulates an inflammation-sensitive signaling checkpoint in macrophages. *Elife* 4, (2015).

28. C. L. Abram, G. L. Roberge, L. I. Pao, B. G. Neel, C. A. Lowell, Distinct roles for neutrophils and dendritic cells in inflammation and autoimmunity in moth-eaten mice. *Immunity* 38, 489-501 (2013).
29. K. J. Eash, A. M. Greenbaum, P. K. Gopalan, D. C. Link, CXCR2 and CXCR4 antagonistically regulate neutrophil trafficking from murine bone marrow. *J Clin Invest* 120, 2423-2431 (2010).
30. E. Balish *et al.*, Mucosal and systemic candidiasis in IL-8R α ^{-/-} BALB/c mice. *J Leukoc Biol* 66, 144-150 (1999).
31. S. R. Wu, P. Reddy, Regulating Damage from Sterile Inflammation: A Tale of Two Tolerances. *Trends in immunology* 38, 231-235 (2017).

Acknowledgments: We are grateful to C. Reis e Sousa and C. A. Lowell for sharing essential reagents. We thank C. Reis e Sousa and members of the D.S. laboratory for discussions and critical reading of the manuscript. We appreciate R. Mota for his advice on the pancreatitis model. We thank the staff at the CNIC facilities for technical support.

Funding: C.d.F. is supported by AECC Foundation as recipient of an “Ayuda Fundación Científica AECC a personal investigador en cancer”. P.S.L. is funded by grant BES-2015-072699 from Spanish Ministerio de Ciencia, Innovación y Universidades (MCIU). M.E. is the recipient of a CNIC International PhD Programme fellowship “la Caixa”-Severo Ochoa OSLC-CNIC-2013-04. S.K.W. is supported by a European Molecular Biology Organization (EMBO) Long-term Fellowship (grant ALTF 438-2016) and a CNIC-International Postdoctoral Programme Fellowship (grant 17230-2016). Work in the D.S. laboratory is funded by the CNIC and grant SAF2016-79040-R from MCIU, Agencia Estatal de Investigación and Fondos Europeos de Desarrollo Regional (FEDER); B2017/BMD-3733 Immunothercan-CM from Comunidad de Madrid; RD16/0015/0018-REEM from FIS-Instituto de Salud Carlos III, MICINN and FEDER; Acteria Foundation; Constantes y Vitales prize (Atresmedia); La Marató de TV3 Foundation (201723); the European Commission (635122-PROCROP H2020) and the European Research Council (ERC-2016-Consolidator Grant 725091). The CNIC is supported by the MCIU and the Pro-CNIC Foundation, and is a Severo Ochoa Center of Excellence (SEV-2015-0505).

Author contributions: Conceptualization: C.d.F., P.S-L., and D.S.; Methodology, Investigation, Analysis and Validation: C.d.F., P.S-L, M.E., S.K.W., S.M-C, N.B-M, O.S., M.G., and F.M.; Resources: O.S., E.C., and A.P.; Writing original draft: C.d.F., P.S-L., and D.S.; Editing draft: all authors; Supervision, Project administration and Funding acquisition: D.S.

Competing interests: The authors have declared that no conflict of interest exists.

Data and materials availability: All data to understand and assess the conclusions of this research are available in the main text and supplementary materials.

Supplementary Materials

Materials and Methods

Figures S1-S13

Figure legends

Fig. 1. DNNGR-1 regulates neutrophil infiltration and tissue damage during acute pancreatitis. (A) Acute pancreatitis was induced by intraperitoneal injection of caerulein hourly for 6 hours in WT and DNNGR-1-deficient (*Clec9a^{gfp/gfp}*) mice. PBS injection was used as control. Animals were analyzed 12 hours after the last injection. (B) Infiltrating neutrophils (left) and monocytes (right) in pancreas quantified by flow cytometry. (C, D) Anti-DNNGR-1 or isotype control antibodies were intraperitoneally injected in WT (C) or WT and *Batf3^{-/-}* (D) mice on days -1 and 0. Infiltrating neutrophils in pancreas quantified by flow cytometry. (E) Levels of lipase were detected in serum from peripheral blood. (F) Hematoxylin and eosin (H&E) staining in pancreatic sections (left). Representative images of n=5 pancreata per experimental condition. Percentages of edematous area (right). (G, H) *Rag1^{-/-}* and *Rag1^{-/-} Clec9a^{gfp/gfp}* mice were subjected to pancreatitis as indicated in (A). (G) Infiltrating neutrophils in pancreas quantified by flow cytometry. (H) Serum lipase. (B-H) Each dot represents a single mouse. Mean±SEM of a representative experiment (N≥2). Significance was assessed by unpaired Student's *t*-test between genotypes (B, E-H) or treatments (C,D); **p*<0.05; ***p*< 0.01.

Fig. 2. DNNGR-1 controls neutrophil recruitment and pathology associated to systemic candidiasis. *Candida albicans* was intravenously injected in WT and *Clec9a^{gfp/gfp}* mice. (A) Weight loss and (B) survival rate were recorded. After 6 days post-infection: (C) renal fungal burden (d.l.: detection limit), (D) renal infiltrated neutrophils (left) and monocytes (right) quantified by flow cytometry, (E) H&E staining (arrows indicate neutrophil accumulation). (F,G) anti-DNNGR-1 or isotype control antibodies were intraperitoneally injected in WT (F) or

WT and *Batf3*^{-/-} (G) mice on day -1 and daily after infection; infiltrating renal neutrophils were analyzed by flow cytometry. (H,I) *Rag1*^{-/-} and *Rag1*^{-/-}*Clec9a*^{gfp/gfp} mice were infected as indicated. (H) Renal neutrophils (day 6 post-infection) quantified by flow cytometry and (I) survival rate. (J) DAPI and TUNEL staining in renal sections (left) and percentage of TUNEL-positive cells (right), (K) Serum creatinine and (L) Kidney injury molecule-1 (Kim-1) relative expression in total kidney in WT and *Clec9a*^{gfp/gfp}-infected mice. (M) Renal neutrophils and (N) Kim-1 expression in total kidney at the indicated times post-infection. (A,C,D,F-H,M) Mean±SEM of a representative experiment (N≥2) including at least 5 mice/condition. (B,I) Representative experiment (N≥2) with n≥9 mice per genotype. (C,D,F-H,K,M) Each dot represents a single mouse. (E,J) Representative images of n≥5 kidneys per condition. (K,L,N) Mean±SEM of ≥2-pooled experiments (n≥5 per condition). Significance was assessed by 2-way ANOVA with Bonferroni post-hoc test (A), log-rank (B,I) or unpaired Student's *t*-test between genotypes (C,D,H,J-N) or treatments (F,G); **p*<0.05; ***p*<0.01; ****p*<0.001.

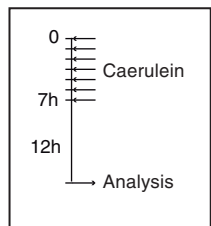
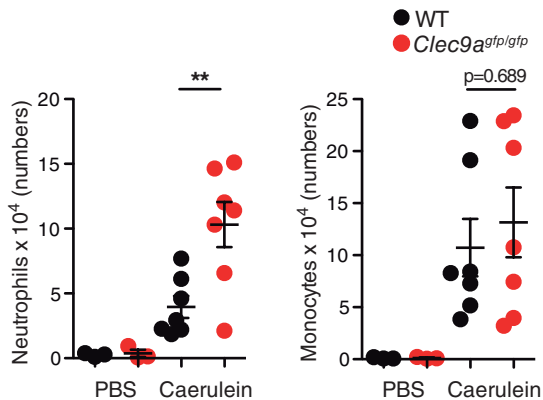
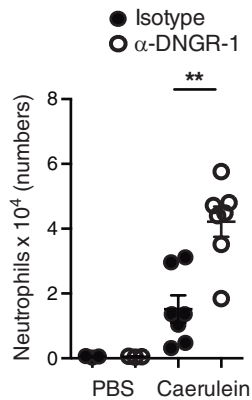
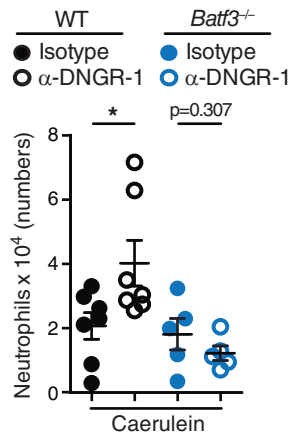
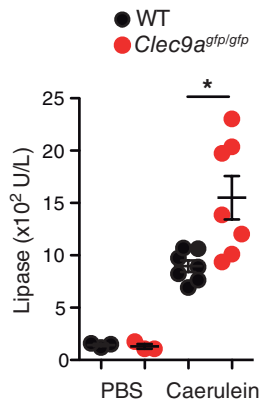
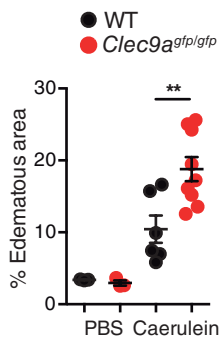
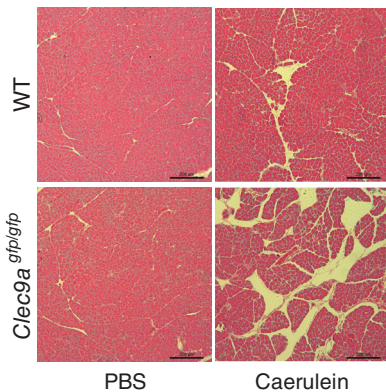
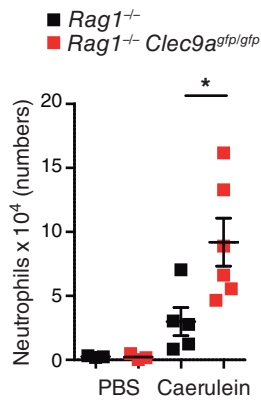
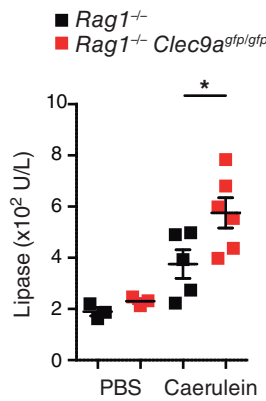
Fig. 3. DNGR-1 restrains tissue damage by dampening neutrophil-mediated

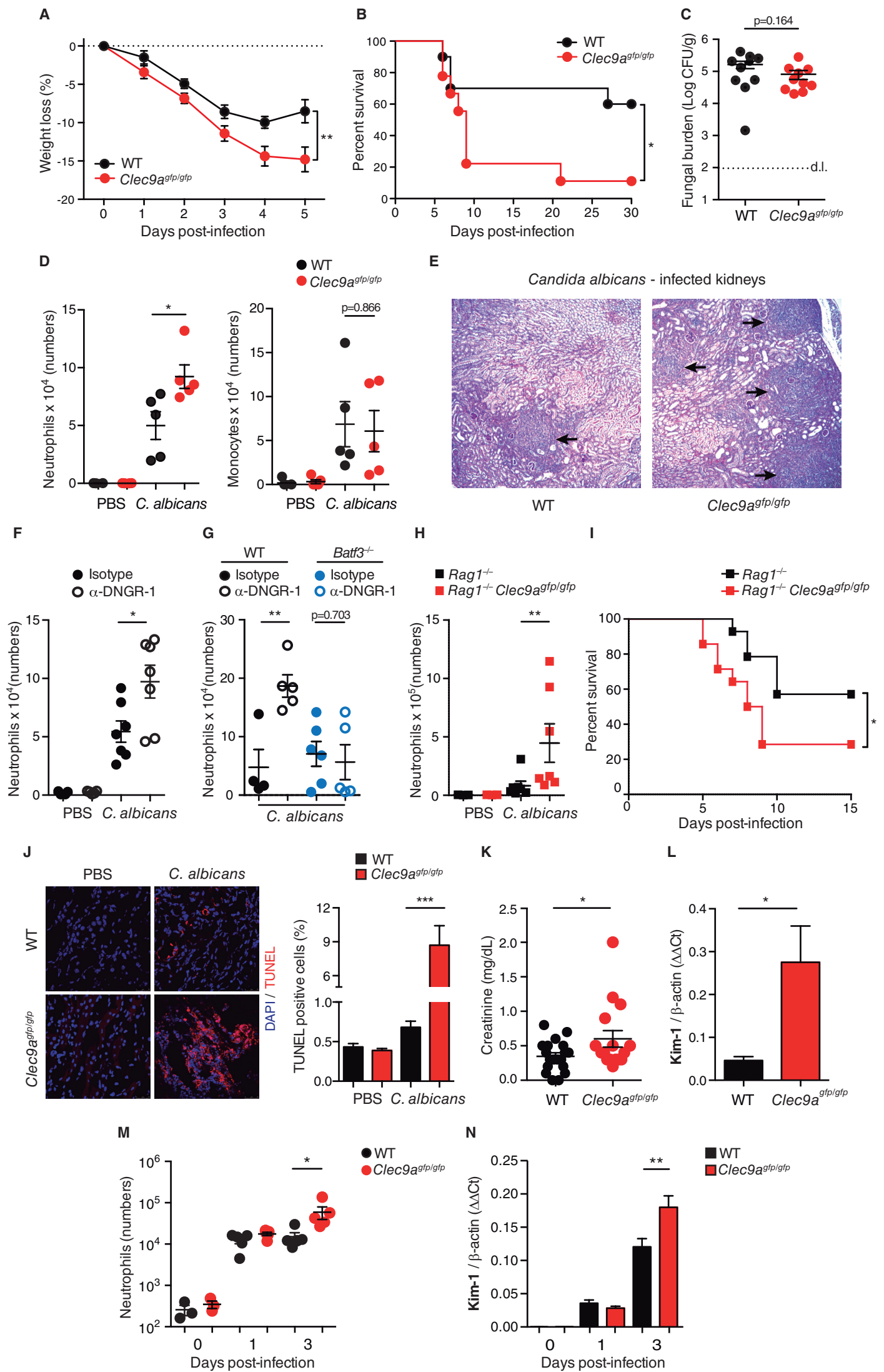
immunopathology. (A) Representative scheme of pancreatitis induction. 1A8 neutrophil-depleting antibody or isotype-control were administered intraperitoneally (i.p.) as indicated. (B) H&E staining in pancreatic sections (left) and percentages of edematous area (right). Representative images of n≥6 pancreas per experimental condition. (C) Representative scheme of *C. albicans* infection; fungizone or PBS together or not with 1A8 or isotype-control were i.p. administered as indicated. (D-I) *C. albicans* was intravenously injected in WT and *Clec9a*^{gfp/gfp} mice. After 6 days post-infection: (D,F) Renal infiltrating neutrophils quantified by flow

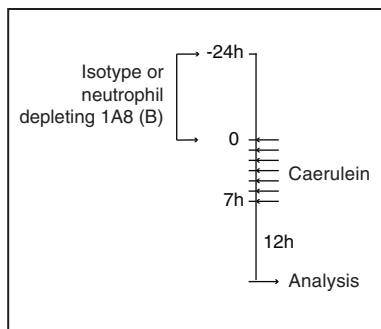
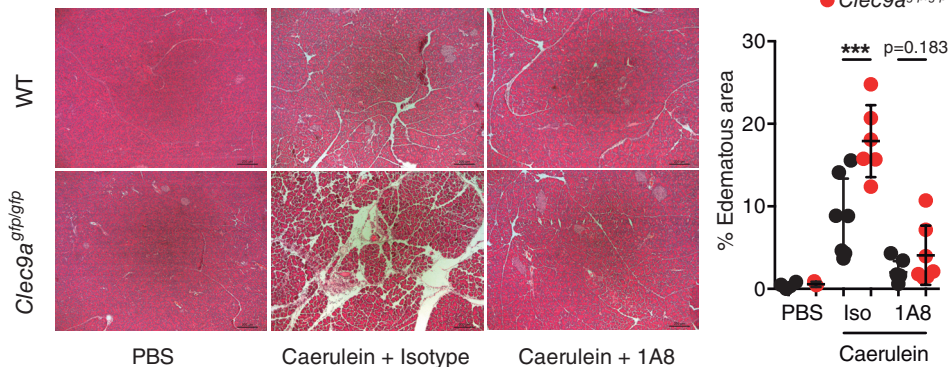
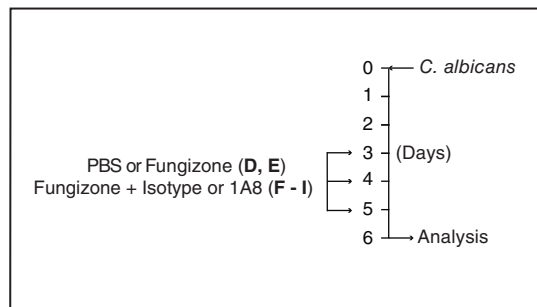
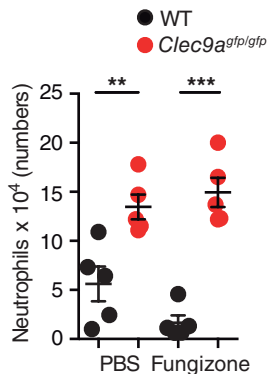
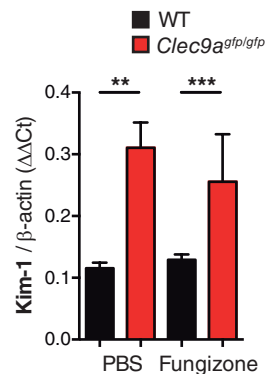
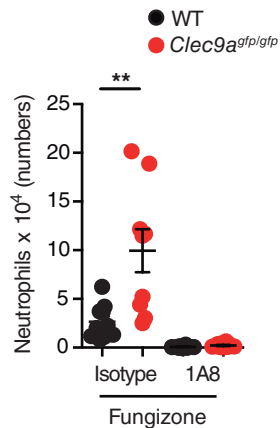
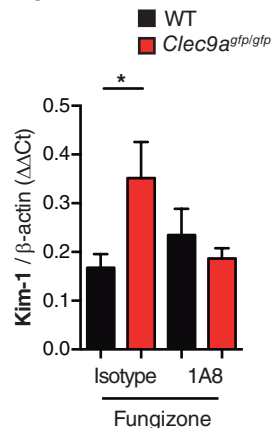
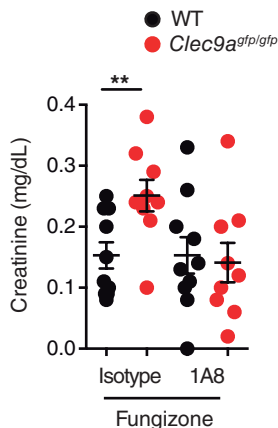
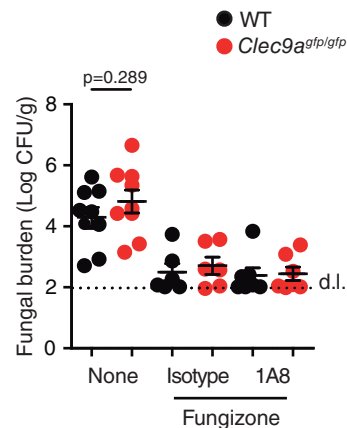
cytometry and (E,G) Kim-1 expression in total kidney, (H) Serum creatinine and (I) Renal fungal burden (d.l.: detection limit). (B,D-I) Mean±SEM of a representative experiment (N≥2) including at least 5 mice per condition. Each dot represents a single mouse. Significance was assessed by unpaired Student's *t*-test between genotypes; **p*<0.05; ***p*<0.01; ****p*<0.001.

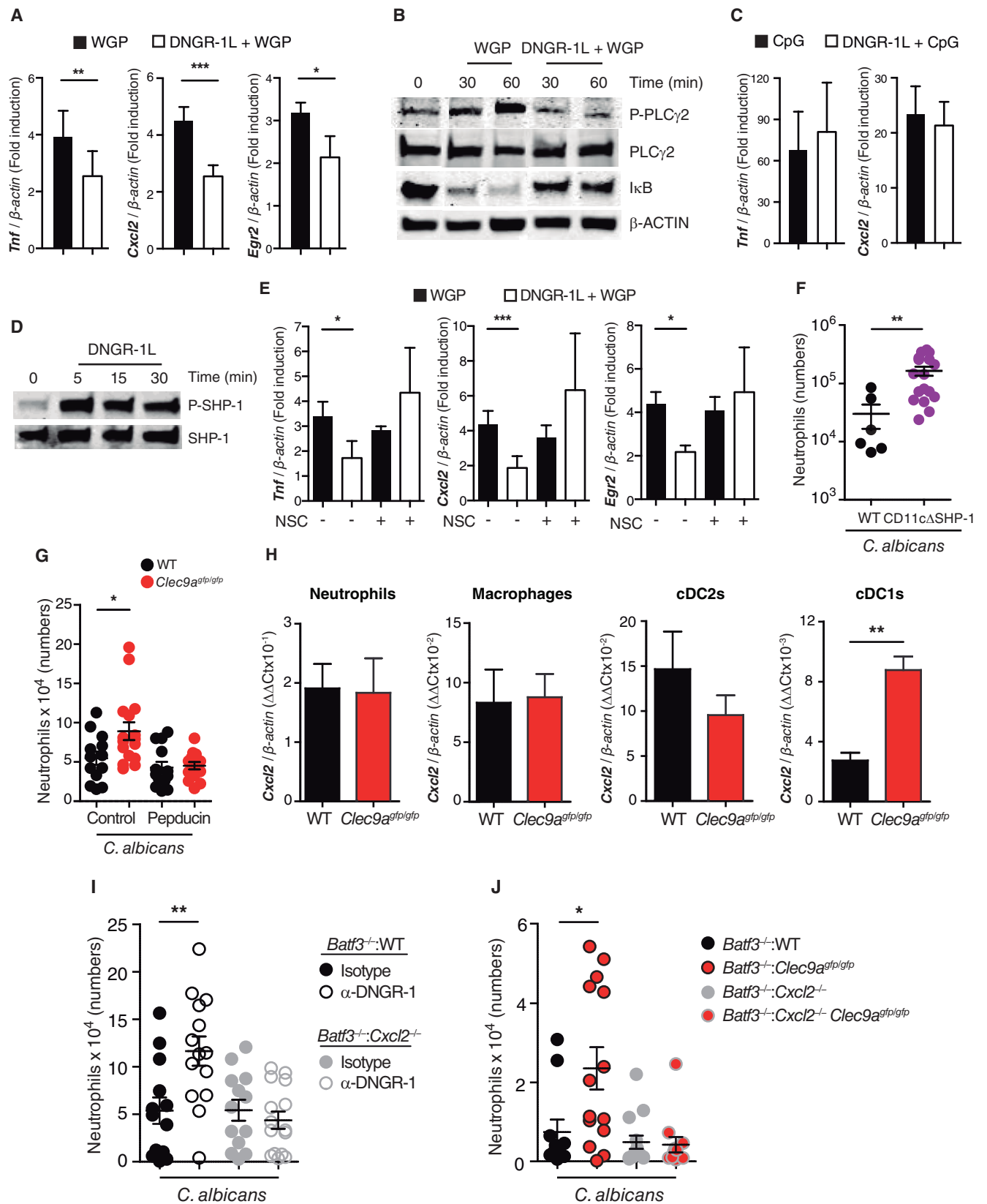
Fig. 4. DNGR-1 activates SHP-1 and controls neutrophil infiltration by dampening Mip-2 expression in cDC1s. (A-E) MutuDCs untreated or exposed to DNGR-1 ligand (DNGR-1L), were stimulated with whole glucan particles (WGP) or CpG where indicated. (A) *Tnf*, *Cxcl2* and *Egr2* expression by qPCR after 4 hours of stimulation, fold induction versus non-stimulated cells. (B) Immunoblot analysis with the indicated antibodies. (C) *Tnf* and *Cxcl2* expression as in (A). *Egr2* expression was not induced in response to CpG. (D) MutuDCs exposed to DNGR-1L and analyzed by immunoblot. (E) *Tnf*, *Cxcl2* and *Egr2* expression in cells pre-incubated with the SHP-inhibitor NSC-87877 (NSC) and stimulated as in (A). (F-J) Mice were intravenously infected with *C. albicans*. (F,G,I,J) Renal infiltrating neutrophils were quantified after 6 days in the indicated mice. (F) *Itgax*^{+cre}*Ptpn6*^{fl/fl} (CD11cΔSHP-1) and WT littermates. (G) Pepducin or control peptide-treated WT and *Clec9a*^{gfp/gfp} mice. (H) Relative *Cxcl2* expression by immune cells in the kidney 60 hours post-infection. (I) Lethally irradiated B6/SJL CD45.1 recipient mice were reconstituted with 50% of *Batf3*-deficient BM cells (CD45.2, producing Mip-2 but lacking cDC1s) and 50% of Mip-2-deficient BM cells (CD45.2, *Cxcl2*^{-/-} mice). Thus, *Batf3*^{-/-}:*Cxcl2*^{-/-} chimeric mice are defective for Mip-2 production only in cDC1s compared with control BM chimeras (*Batf3*^{-/-}:WT). Anti-DNGR-1 or isotype control antibodies were intraperitoneally injected on day -1 and daily after infection. (J) The following mixed BM chimeric mice were

generated as in I: 1) *Batf3*^{-/-}:WT control chimeras; 2) *Batf3*^{-/-}:*Clec9a*^{gfp/gfp}, which generate cDC1s lacking DNNGR-1; 3) *Batf3*^{-/-}:*Cxcl2*^{-/-}, which produce Mip-2-deficient cDC1s; and 4) *Batf3*^{-/-}:*Clec9a*^{gfp/gfp} *Cxcl2*^{-/-}, which generate cDC1s lacking both DNNGR-1 and Mip-2. (I,J) All cDC1s in the kidney were of donor origin (fig. S12A, C), and the number of reconstituted cDC1s were equal in the different chimeric mice (fig. S12B, D). (A,C,E,H) Mean+SEM of pooled experiments including N≥3 individual cultures or ≥4 mice per condition (N≥4). (B,D) Representative immunoblots (N≥2). (F,G,I,J) Mean±SEM of 2 pooled experiments. Each dot represents a single mouse. Significance was assessed by paired Student's *t*-test between DNNGR-1L-treated or not (A,C,E) or genotypes (H) or unpaired between genotypes (F,G,I,J); **p* < 0.05; ***p* < 0.01; ****p*<0.001.

A**B****C****D****E****F****G****H**



A**B****C****D****E****F****G****H****I**



Science



Supplementary Materials for

DNGR-1 in DCs limits tissue damage by dampening neutrophil recruitment

Authors: Carlos del Fresno^{1, ‡, *}, Paula Saz-Leal^{1, ‡}, Michel Enamorado¹, Stefanie K. Wculek¹, Sarai Martínez-Cano¹, Noelia Blanco-Menéndez¹, Oliver Schulz², Mattia Gallizioli³, Francesc Miró³, Eva Cano⁴, Anna Planas^{3,5}, David Sancho^{1,*}

Affiliations:

¹ Immunobiology Laboratory. Centro Nacional de Investigaciones Cardiovasculares (CNIC), Madrid, Spain

² Immunobiology Laboratory, The Francis Crick Institute, London, UK

³ Institut d'Investigacions Biomèdiques August Pi i Sunyer (IDIBAPS), Barcelona, Spain

⁴ Chronic Disease Programme-CROSADIS, Instituto De Salud Carlos III, Madrid, Spain

⁵ Department of Brain Ischemia and Neurodegeneration, Institut d'Investigacions Biomèdiques de Barcelona (IIBB-CSIC), Barcelona, Spain

M.E. current address: Mucosal Immunology Section, Laboratory of Parasitic Diseases, NIAID, NIH, Bethesda, MD 20892, USA

*Correspondence to:

David Sancho

Carlos del Fresno

Centro Nacional de Investigaciones Cardiovasculares Carlos III (CNIC)

Melchor Fernández Almagro, 3

E-28029, Madrid, Spain

Tel: (+ 34) 914531200 Ext 2010

Tel (direct line): (+ 34) 662 990 4777 2010

FAX: (+ 34) 914531245

E-mail:

dsancho@cnic.es

cdelfresno@cnic.es

‡ Co-first authors

This PDF file includes:

Materials and Methods
Figs. S1 to S13

Materials and Methods

Reagents and *Candida albicans*

Reagents used were as follows: Caerulein (Sigma), anti-DNGR-1 blocking antibody (7H11, BioXCell), anti-Ly6G antibody (1A8, BioXCell) and their polyclonal rat IgG isotype controls (Sigma); Fungizone (Amphotericin B, Whittaker Bioproducts); CpG (ODN 1668, Sigma), Whole Glucan Particles (WGP, Biothera), NSC-87877 (SHP inhibitor, Calbiochem), pepducin and control peptides (Genescript) and cefovecin antibiotic (Zoetis). High-binding ligand for DNGR-1 (DNGR-1L) is a combination of F-actin and myosin II kindly provided by Dr. C. Reis e Sousa (20).

Candida albicans (strain SC5314, kindly provided by Prof. C. Gil, Complutense University, Madrid) was grown on YPD-agar plates (Sigma) at 30°C for 48h. Heat-killed *C. albicans* (HKC) was prepared by boiling for 30 minutes.

Mouse strains and cells

Mouse colonies (6 – 12 weeks old), were all on a C57BL/6 background and bred at CNIC under specific pathogen-free conditions. They included WT, *Clec9a^{gfp/gfp}* (DNGR-1-deficient, B6(Cg)-*Clec9atm1.1Crs/J*) (7), *Batf3^{-/-}* (B6.129S(C)-*Batf3^{tm1Kmm}/J*, The Jackson Laboratory), *Rag1^{-/-} Clec9a^{gfp/gfp}*, which were generated by crossing *Rag1^{-/-}* (B6.129S7-*Rag1tm1Mom/J*, The Jackson Laboratory) with *Clec9a^{gfp/gfp}* mice; *Ptpn6^{n/n}Itgax^{+/+}* and *Ptpn6^{n/n}Itgax^{Cre/+}* kindly provided by Prof. Clifford A. Lowell, UCSF, San Francisco, CA (CD11cΔSHP-1, bred as littermates) (28); and *Cxcl2^{-/-} Clec9a^{gfp/gfp}*, which were generated by crossing *Cxcl2^{-/-}* (MIP-2-deficient, C57BL/6NJ-*Cxcl2^{em1(IMPC)/J}*) with *Clec9a^{gfp/gfp}* mice. Mice expressing the CD45.1 allele (B6.SJL-*Ptprc^aPepc^b*/BoyJ, The Jackson Laboratory) were used as recipients for mixed bone marrow chimeras. Experiments were conducted with sex- and age-matched mice. Experiments were approved by the animal ethics committee at CNIC and conformed to Spanish law under Real Decreto 1201/2005. Animal procedures were also performed in accordance to EU Directive 2010/63EU and Recommendation 2007/526/EC.

B3Z cells (kindly provided by Prof. N. Shastri, University of California, Oakland) express a β-gal reporter for nuclear factor of activated T cells (NFAT) (7). B3Z cells stably transduced with mouse *Clec9a* and *Syk* (B3Z-mDNGR-1-Syk cells) allow the detection of DNGR-1 ligands by testing their agonistic capacity through NFAT reporter activation and induction of β-gal activity. Cells were cultured in RPMI 1640 supplemented with 2 mM L-glutamine, 100 U/ml penicillin, 100 μg/ml streptomycin, 50 μM 2-mercaptoethanol, and 10% heat-inactivated fetal bovine serum (FBS) (all from Life Technologies, Carlsbad, CA) at 37°C and regularly checked for the absence of mycoplasma. Reporter assays were carried out in serum-free AIM-V medium (Life technologies). Non-transduced B3Z or B3Z-mDNGR-1-Syk cells were incubated with plated DNGR-1L at the indicated concentrations. If needed, cells were pre-incubated for 30 min with 20 μg/ml of 7H11 (or isotype-matched control). After overnight culture, LacZ activity was measured lysing cells in CPRG (Roche, Basel, Switzerland)-containing buffer. 1-4 hours later, O.D. 595 was measured relative to O.D. 655 nm used as a reference.

The MutuDC1940 line (MutuDCs), kindly provided by Prof. H. Acha-Orbea, (University of Lausanne, Lausanne, Switzerland) was kept in culture and harvested at ≈ 90% of confluence as described (20). Cells were plated on RIA plates (Corning) in the presence or not of DNGR-1L (0.1 μM) for 5 minutes and subsequently stimulated with HKC (10:1 ratio), WGP (150 μg/ml) or CpG (0.5 μg/ml) for given times. In cases without further stimulation, MutuDCs were plated with DNGR-1L for indicated times. When required, MutuDCs were pre-incubated before

stimulation for 30 min with either 20 μ M of the SHP inhibitor NSC-87877, 7H11 antibody (250 μ g/ml), or isotype-matched control.

In vivo models

For *Candida albicans* systemic infections, mice were intravenously (i.v.) infected with 10^5 *C. albicans* in sterile phosphate buffered saline (PBS, Life Technologies) and monitored daily for weight, general health, and survival, following the institutional guidance. Control mice were given PBS. Fungizone was intraperitoneally (i.p.) administered (2 mg/kg body weight in PBS) daily from day 3 post-infection (p.i.) onwards. Pepducin and corresponding control peptides were subcutaneously (s.c.) injected daily, starting at day 3 p.i. Unless otherwise specified, animals were culled at day 6 p.i.

Kidney fungal burden was determined by plating organ homogenates obtained mechanically over 70- μ m cell strainers (BD Biosciences) after slicing the tissue, in serial dilutions on YPD agar plates. Colony-forming units (CFU) were counted after growth at 30°C for 48 h.

To obtain cell suspensions for flow cytometry, kidneys were digested with Liberase TL (Roche) for 10 minutes at 37°C and filtered through 70- μ m cell strainers (BD Biosciences). For the isolation of bone marrow cells (BM), femurs were collected and flushed. In all cases, red blood cells were lysed using RBC Lysis Buffer (Sigma) for 3 minutes at room temperature (RT). Washes and phenotypic analysis of leukocytes were performed on ice-cold FACS Buffer (PBS supplemented with 5 mM EDTA and 3% FBS).

For quantitative PCR analysis of Kim-1 expression, RNA was purified from total kidneys.

Neutrophil counts in blood and creatinine levels from serum samples were determined by the Biochemical Analysis unit at CNIC.

In experiments addressing cytokine expression *in vivo*, both kidneys from at least four mice per group were harvested at day 2.5 (60 hours) p.i. and processed as described. Leukocytes were enriched by Percoll centrifugation (Sigma) (40% in HBSS, 300 x g, 30 minutes, RT) and populations were isolated by cell sorting.

Caerulein-induced acute pancreatitis was induced by seven intraperitoneal injections of caerulein (50 μ g/kg body weight in PBS at intervals of 1 h). Control mice were given PBS. All animals were sacrificed 12 h after the last injection of caerulein. Pancreas and BM were processed as described above. Flow cytometric analysis of pancreas immune infiltrates was also performed on cell suspensions as indicated before. Neutrophil count in blood and serum lipase levels were measured by the Biochemical Analysis unit at CNIC.

When necessary, mice were treated i.p. with 100 μ g of 7H11 anti-DNGR-1 blocking (BioXCell) antibody or isotype-matched control. For acute pancreatitis, mice were injected on days -1 and 0. In the case of *C. albicans* infection, injections were administered daily from day -1 to sacrifice.

In neutrophil-depleting experiments, mice were treated i.p. with anti-Ly6G antibody (clone 1A8 (BioXCell), 25 μ g per injection and mouse in PBS) or isotype-matched control. In acute pancreatitis, mice were injected on days -1 and 0. For the *C. albicans* infection model, antibodies were administered daily, starting at day 3 post-infection.

Generation of mixed bone marrow chimeras

CD45.1 lethally irradiated (5.5 Gy, twice) mice were i.v. reconstituted with up to 5×10^6 of total bone marrow cells in PBS consisting of 50:50 mixtures of *Batf3*^{-/-}:WT, *Batf3*^{-/-}

:*Clec9a*^{gfp/gfp}, *Batf3*^{-/-}:*Cxcl2*^{-/-} or *Batf3*^{-/-}:*Cxcl2*^{-/-} *Clec9a*^{gfp/gfp}. Mice were subcutaneously injected with cefovecin (30 mg/kg body weight in PBS). Blood was collected 3 weeks later, lysed and stained on ice-cold FACS Buffer to check reconstitution. One week later, mice were i.v. infected with 7×10^4 *C. albicans*, due to increased susceptibility to the fungus of *Batf3*^{-/-}:WT control chimeric mice compared with regular (non-irradiated) WT mice. Mice were monitored and culled as described above.

Antibodies and flow cytometry

Samples were stained with the appropriate antibody cocktails in ice-cold FACS Buffer. Antibodies included biotinylated anti-DNGR-1 (7H11), Alexa647-anti-Dectin-1 (2A11, AbD Serotec, Kidlington, UK), FITC-anti-Ly6C (AL-21), FITC or PECy7-anti-CD11b (M1/70), PeCy7, PercPCy5.5 or APC-anti-CD11c (HL3), PE-anti-Ly6G (1A8) and Brilliant Violet 421-anti-B220 (RA3-6B2) from BD Pharmingen (San Diego, CA); PercPCy5.5-anti-CD45 (30-F11), PercPCy5.5-anti-CD45.2 (104), APC-anti-CD45.1 (A20) and APC or PE-streptavidin from eBioscience (Hatfield, UK); Violet Fluor 450 anti-CD3 (17A2) from TONBO Bioscience (San Diego, CA) and PE-anti-XCR1 (ZET) from Biolegend (San Diego, CA). Dead cells were excluded by Hoechst 33258 (Invitrogen, Carlsbad, CA) incorporation. Purified anti-FcγRIII/II (2.4G2, TONBO Bioscience) was used to block Fc-receptors at 4°C for 10 minutes in all the stainings. Regarding immune infiltration analysis, monocytes were defined as Hoechst⁻ CD45⁺CD11b⁺Ly6C^{+/bright}Ly6G⁻ and neutrophils as Hoechst⁻CD45⁺CD11b⁺Ly6C⁺Ly6G⁺. Reconstitution of mixed bone marrow chimeras was assessed by checking CD45 allotype of neutrophils. Events were acquired using LSRFortessa flow cytometer (BD).

For cell sorting, Percoll-enriched leukocytes were labelled with FITC-anti-CD19 (1D3), Alexa 647-anti-CD3 (17A2), PeCy7-anti-CD11c (HL3), APCCy7-anti-CD11b (M1/70), FITC-anti-Ly6C, PercPCy5.5-anti-SiglecF (E50-2440), PE-anti-Ly6G and Alexa 647-anti-CD64 (X54-5/7.1) from BD Pharmingen; Brilliant Violet 570-anti-CD45 (30-F11) and PE-anti-XCR1 from Biolegend; PercPCy5.5-anti-CD127 (A7R34) and PE-anti-NK1.1 (PK136) from TONBO Bioscience; biotinylated anti-CD172a (Sirpα) (P84), PercPCy5.5-streptavidin from eBioScience and Hoechst 33258. It was followed by flow cytometric sorting of CD45⁺CD11b⁺Ly6G⁺ (neutrophils), CD45⁺CD11b⁺Ly6G⁻CD64⁺ (macrophages), CD45⁺CD11b⁻CD11c⁺XCR1⁺ (cDC1s), CD45⁺CD11b⁺Ly6G⁻CD64⁻CD11c⁺Sirpα⁺ (cDC2s), CD45⁺CD11b⁺Ly6G⁻CD64⁻Sirpα⁻Ly6C^{+/bright} (monocytes), CD45⁺CD3⁺ (T cells), CD45⁺CD19⁺ (B cells), CD45⁺CD3⁻CD19⁻NK1.1⁺ (NK cells), CD45⁺CD3⁻CD19⁻NK1.1⁻CD127⁺ (ILCs) and CD45⁺Ly6G⁻SiglecF⁺ (eosinophils), Hoechst⁻ populations (see fig. S10) on FACS Aria SORP (BD) or Sy3200 (Sony Biotechnology) flow sorters. Data were analyzed with FlowJo software (Tree Star).

Histopathology and TUNEL staining

Kidneys or pancreas were fixed in 4% PFA (Thermo Fisher Scientific, Waltham, MA) until processed by the Histopathology unit at CNIC. Samples were dehydrated with ethanol, embedded in paraffin and sections (3-5-μm thickness) were stained with hematoxylin and eosin (H&E, Sigma) following standard protocols. Tissue sections were visualized under a Leica DM2500 microscope (Leica Microsystems, Solms, Germany) and quantification was performed using ImageJ software (Bitplane, Belfast, UK).

For cell death assay by TUNEL staining, renal samples were fixed with 4% PFA and embedded in O.C.T. (Tissue-Tek, Torrance, CA) for cryosectioning. *In situ* detection of cells with DNA-strand breaks was performed on sections (5 μm) by the TUNEL (terminal

deoxynucleotidyl transferase dUTP nick end labelling) staining method using the In Situ Cell Death Detection Kit (Roche) according to manufacturer's instructions. Sections were counterstained with 4', 6-diamidino-2-phenylindole (DAPI, Eugene, OR). Confocal images were obtained with a Leica TCSSP5 confocal scanning laser unit attached to an inverted epifluorescence DMI6000B microscope fitted with an HCX PL APO lambda blue 63X/1.4 NA oil immersion objective, using Las-AF acquisition software (Leica). For image processing and analysis, two channels were used for the analysis: C1_DAPI (blue) and C2_TUNEL (red). A total of 150 images with two channels each were processed by using custom-designed algorithms within Definiens Developer XD software (Definiens AG, München, Germany). TUNEL positive nuclei were determined by applying a red threshold of 80. Every nucleus showing a mean value of the C2_TUNEL superior to 80, in a ring region with a dilation of two pixels, was classified as positive. Percentage of TUNEL positive cells was calculated by plotting TUNEL positive cell number against total cell number (DAPI positive). This processing was performed by the Cellomics Unit at CNIC.

Quantitative-PCR

RNeasy Plus Mini Kit or RNeasy Micro Kit (in case of cell sorting), both from Qiagen (Hilgen, Germany), were used for RNA extraction. cDNA was prepared using the High Capacity cDNA reverse transcription kit (Applied Biosystems, Foster City, CA). Quantitative PCR was performed in a 7900-FAST-384 instrument (Applied Biosystems) by using the GoTaq qPCR master mix from Promega (Madison, WI). Primers used in this work (synthesized by Sigma) were as follows: β -actin Fw: 5'-GGCTGTATTCCCCTCCATCG-3'; β -actin Rv: 5'-CCAGTTGGTAACAATGCCATGT-3'; KIM-1 Fw: 5'-CATATCGTGGAATCACAACGAC-3'; KIM-1 Rv: 5'-ACAAGCAGAAGATGGGCATTG-3'; TNF α Fw: 5'-CCCTCACACTCAGATCATCTTCT-3'; TNF α Rv: 5'-GCTACGACGTGGGCTACAG-3'; MIP-2 Fw: 5'-ACGCCCCCAGGACCC-3'; MIP-2 Rv: 5'-CTTTTGTACCGCCCTTGAGA-3'; EGR-2 Fw: 5'-GTGCCAGCTGCTATCCAGAAG-3'; EGR-2 Rv: 5'-GGCTGTGGTTGAAGCTGGAG-3'. mRNA levels were normalized to β -actin expression. Data are shown as fold induction or relative expression to β -actin ($\Delta\Delta Ct$) as indicated in figure legends.

Immunoblot

Cell lysates were prepared in RIPA buffer containing protease and phosphatase inhibitors (Roche). Samples were run on Mini-PROTEAN TGX PRECAST Gels and transferred onto a nitrocellulose membrane (both from Bio-Rad Laboratories) for blotting with the following antibodies: β -actin (C4) and SHIP-1 (P1C1) from Santa Cruz; PLC γ 2 (MAB3716-SP) from R&D Systems; P- PLC γ 2 (Tyr759, #3874S), I κ B (#9242S), P-SHP-1 (Tyr564, #8849), SHP-1 (#3759), P-SHIP-1 (#3941S) and LYN (#2732), all from Cell Signaling. Alexa Fluor-680- (Life Technologies) or Qdot-800-conjugated (Rockland) secondary antibodies were used and gels were visualized in an Odyssey instrument (LI-COR).

Statistical Analysis

All statistical analyses were performed using Prism software (GraphPad Software). Statistical significance for comparison between two sample groups with a normal distribution (Shapiro–Wilk test for normality) was determined by unpaired two-tailed Student's *t*-test, unless indicated otherwise. In case not following a Gaussian distribution, statistical significance was

established by nonparametric Mann–Whitney test. Comparison of survival curves was carried out by Log-rank (Mantel–Cox) test. For comparison of weight loss evolution, two-way ANOVA tests were performed. Outliers were identified by means of Tukey’s range test. Differences were considered significant at $p < 0.05$ (* $p < 0.05$; ** $p < 0.01$; *** $p < 0.001$). No asterisk indicates non-significant, with some non-significant p-values indicated.

In figure legends, “N” represents the number of independent experiments performed and “n” the number of individual mice included per experiment as indicated.

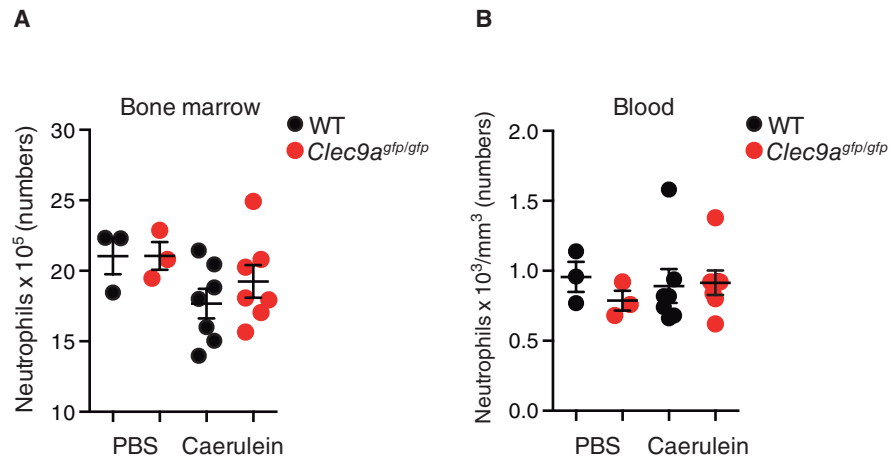


Fig. S1. DNDR-1 does not impact neutrophil count in bone marrow and blood during acute pancreatitis.

Acute pancreatitis was induced by seven intraperitoneal injections of caerulein (50 micrograms/Kg) hourly for 6 hours. PBS injection was used as control. Animals were sacrificed 12 hours after the last injection. Neutrophil count in bone marrow (**A**) (N=3) and blood (**B**) (N=2) were determined in WT and *Clec9a^{gfp/gfp}* mice. Each dot represents a single mouse (n=3-7). Mean±SEM of a representative experiment.

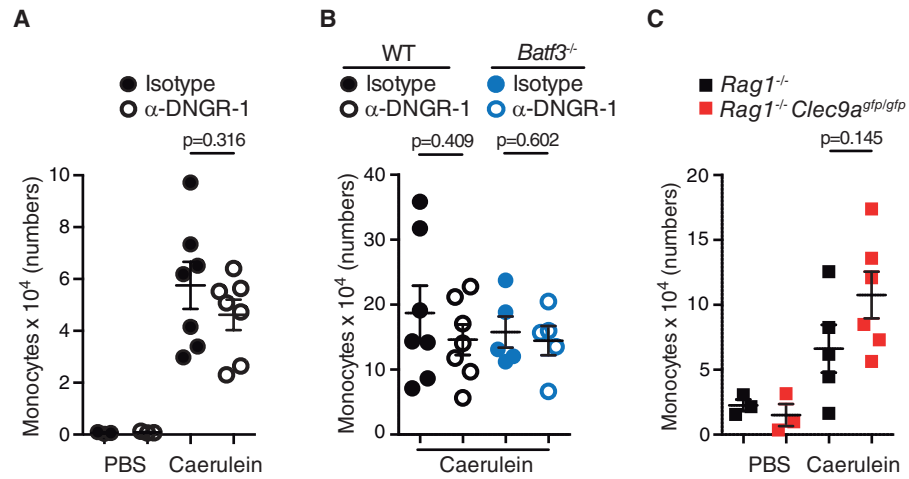


Fig. S2. DNGR-1 does not affect infiltrated monocytes during acute pancreatitis.

Acute pancreatitis was induced by seven intraperitoneal injections of caerulein (50 micrograms/Kg) hourly for 6 hours. PBS injection was used as control when indicated. Animals were sacrificed 12 hours after the last injection. Anti-DNGR-1 or isotype control antibodies were intraperitoneally injected on days -1 and 0 in (A) WT or (B) WT and *Batf3*^{-/-} mice. Infiltrated monocytes were assessed in pancreas by flow cytometry. (N=2) (C) *Rag1*^{-/-} and *Rag1*^{-/-} *Clec9a*^{gfp/gfp} mice were treated with PBS or caerulein as indicated and pancreatic infiltrating monocytes were quantified by flow cytometry (N=3). Each dot represents a single mouse (n=3-7). Mean±SEM of a representative experiment. Significance was assessed by unpaired Student's *t*-test between genotypes (C) or treatments (A, B).

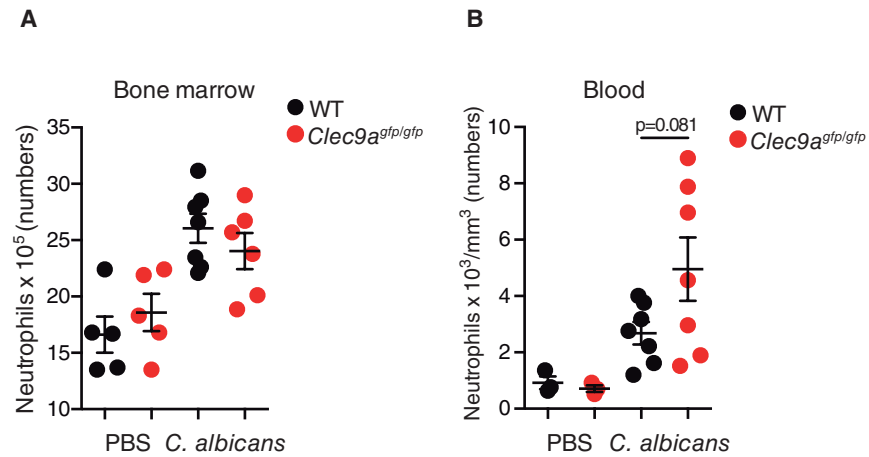


Fig. S3. DNGR-1 does not significantly impact neutrophil count in bone marrow and blood during systemic *Candida albicans* infection.

Mice were intravenously infected with 10⁵ *Candida albicans*. After 6 days, neutrophil count in bone marrow (A) and blood (B) were determined in WT and *Clec9a^{gfp/gfp}* mice. Each dot represents a single mouse (n=3-7). Mean±SEM of a representative experiment (N=2). Significance was assessed by unpaired Student's *t*-test between genotypes.

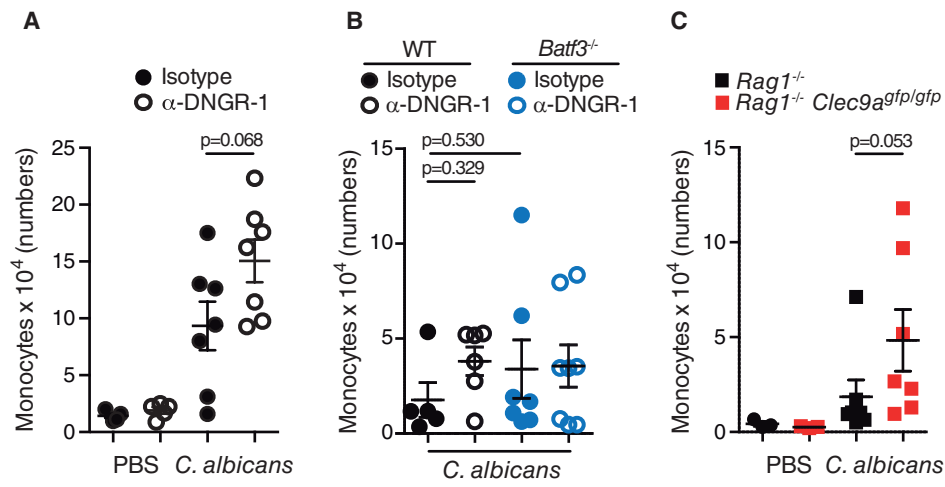


Fig. S4. Monocyte recruitment into *Candida albicans*-infected kidneys is not significantly affected under DNGR-1-deficient conditions.

Mice were intravenously infected with 10^5 *Candida albicans* and infiltrating renal monocytes were analyzed by flow cytometry after 6 days. (A, B) anti-DNGR-1 or isotype control antibodies were intraperitoneally injected in WT (A) (N=3) or WT and *Batf3*^{-/-} (B) (N=2) mice on day -1 and daily after infection. (C) *Rag1*^{-/-} and *Rag1*^{-/-} *Clec9a*^{gfp/gfp} mice were infected as indicated (N=3). Each dot represents a single mouse (n=3-7). Mean \pm SEM of a representative experiment. Significance was assessed by unpaired Student's *t*-test between genotypes (C) or treatments (A, B).

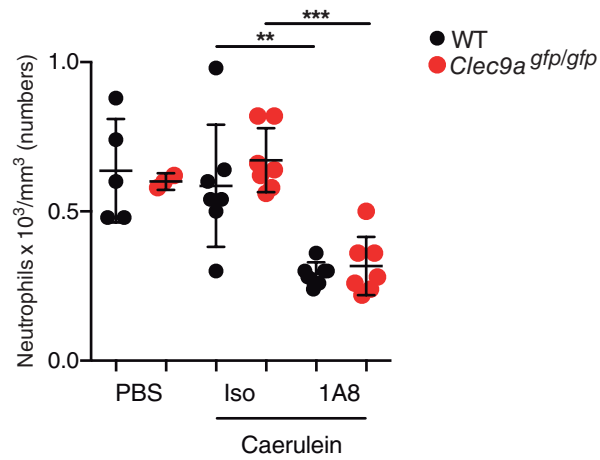


Fig. S5. Efficient 1A8-mediated neutrophil depletion during acute pancreatitis.

Acute pancreatitis was induced by seven intraperitoneal injections of caerulein (50 μ g/Kg) hourly for 6 hours. PBS injection was used as control. On days -1 and 0 (before the first caerulein injection), mice were intraperitoneally injected with anti-Ly6G antibody (clone 1A8, 25 μ g per injection and mouse in PBS) or isotype-matched control. Neutrophil count in blood was performed 12 hours after the last caerulein injection. Each dot represents a single mouse (n=5-7). Mean \pm SEM of a representative experiment (N=2). Significance was assessed by unpaired Student's *t*-test between treatments; ***p*<0.01; ****p*<0.001.

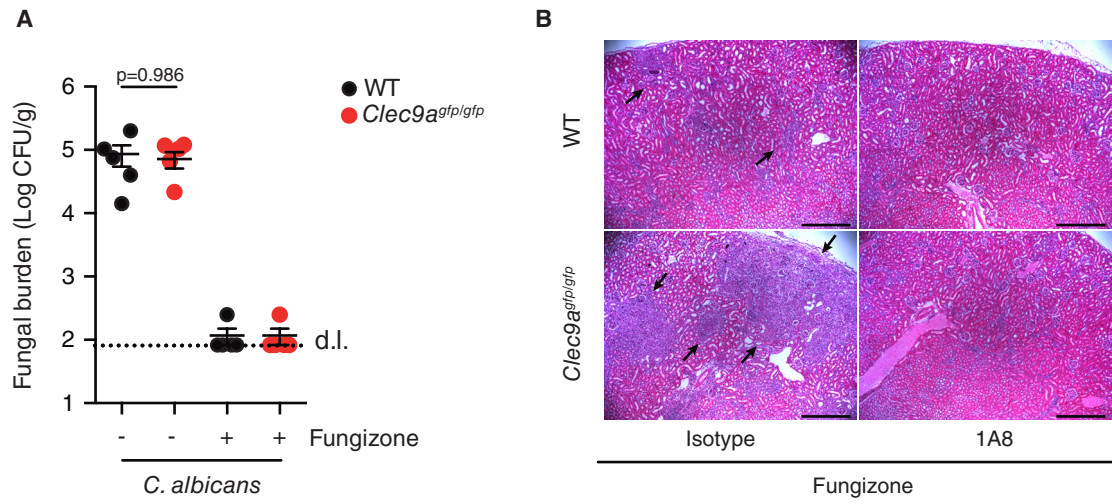


Fig. S6. Effective fungizone-induced elimination of fungal colonization and 1A8-mediated neutrophil depletion in kidney under these conditions during systemic candidiasis.

WT and *Clec9a^{gfp/gfp}* mice were intravenously infected with 10^5 *Candida albicans*. (A) At day 3 post-infection, fungizone (+) (2 mg/kg body weight in PBS) or PBS (-) was intraperitoneally administered daily. After 3 days of treatment, renal fungal burden was determined as Colony Forming Units (CFU) per gram of kidney. d.l.: detection limit. (B) At day 3 post-infection, fungizone was administered together with anti-Ly6G antibody (clone 1A8, 25 μ g per injection and mouse in PBS) or isotype-matched control. After 3 days of treatment, kidneys were collected and H&E staining was performed on renal sections. Arrows indicate neutrophil accumulation. Bar length=200 μ m. (A) Each dot represents a single mouse. Mean \pm SEM of a representative experiment (N=3). Significance was assessed by unpaired Student's *t*-test between genotypes. (B) Representative images of $n \geq 7$ kidneys per condition (N=2).

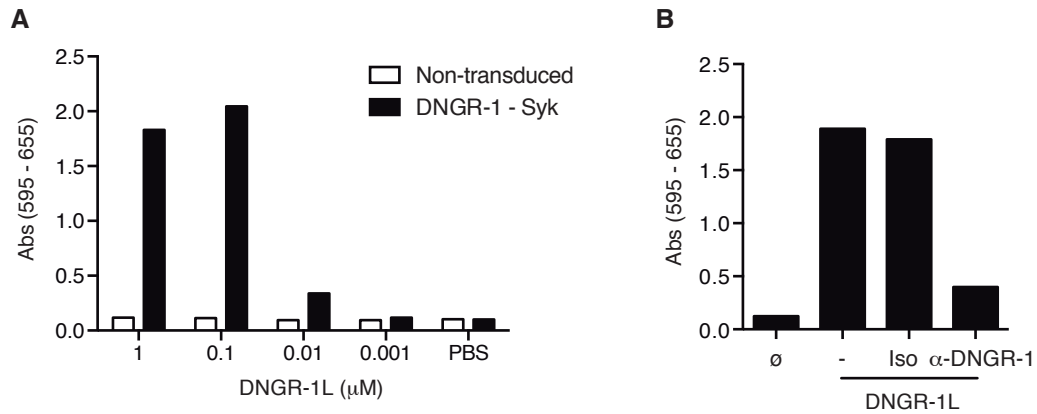


Fig. S7. DNCR-1 ligand efficiently signals through DNCR-1.

(A) B3Z NFAT reporter cells either transduced (DNCR-1-Syk) or not (Non-transduced) with the mouse version of *Clec9a* and *Syk*, were exposed to plated F-actin-based DNCR-1 ligand (DNCR-1L) at the indicated concentrations or to PBS. (B) DNCR-1-Syk B3Z NFAT reporter cells were pre-treated with culture medium (-), isotype control (Iso) or a blocking α -DNCR-1 antibody. After 30 minutes, they were exposed to 0.1 μ M of DNCR-1L or left untreated (\emptyset). (A, B) NFAT reporter activity was revealed by CPRG assay. A representative experiment of a single in vitro culture is shown (N=2).

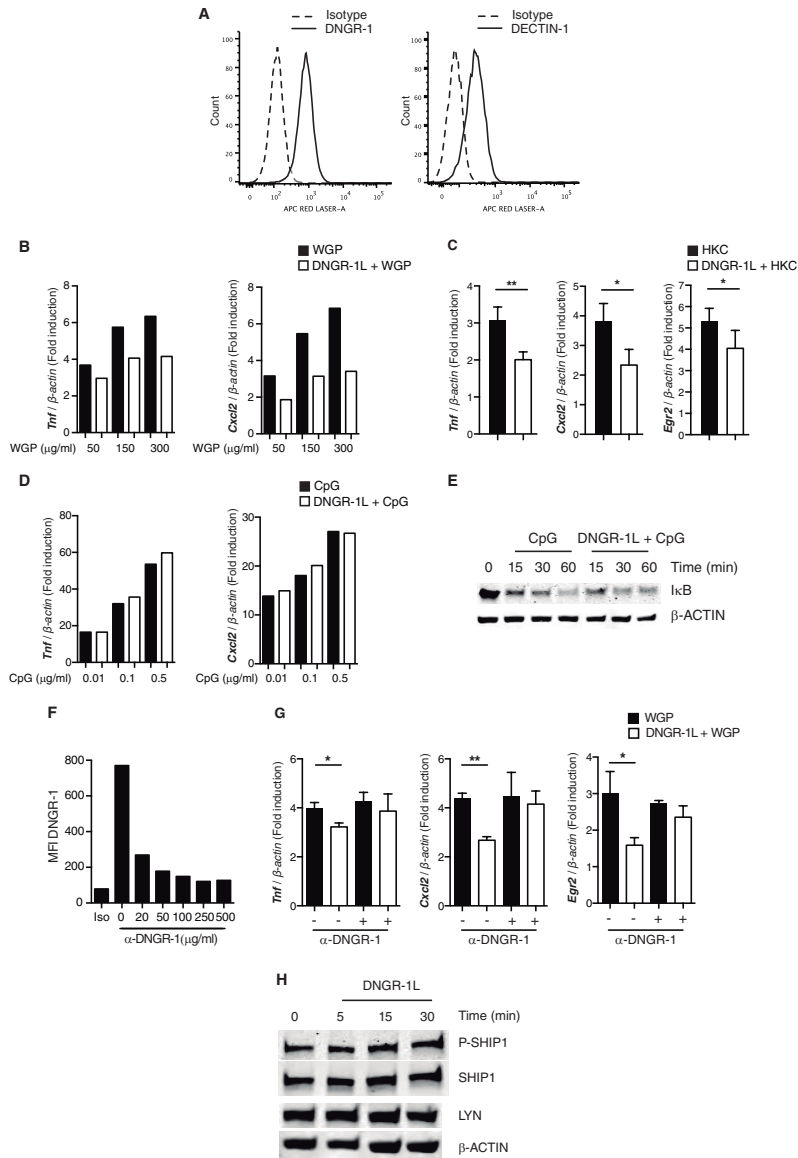


Fig. S8. DNGR-1 ligand triggers specific regulatory responses.

(A) DNGR-1 (left) and DECTIN-1 (right) surface expression was assessed on MutuDC cells by flow cytometry. MutuDCs cultured untreated or exposed to F-actin-myosin II (DNGR-1L), were stimulated with the indicated concentrations of WGP (B), heat-killed *Candida albicans* (HKC) (10:1 ratio) (C) or CpG (D) at the indicated concentrations for 4 hours. *Tnf*, *Cxcl2* and *Egr2* expression was analyzed by Q-PCR and expressed as fold induction versus non-stimulated cells. (E) MutuDCs were exposed or not to DNGR-1L and further stimulated with CpG for the given times. I κ B degradation was analyzed by immunoblot. (F) MutuDCs were pre-treated for 30 minutes with 500 μ g/ml of isotype control (Iso) or the indicated concentrations of a α -DNGR-1 blocking antibody. DNGR-1 surface expression was analyzed afterwards by flow cytometry. Remaining staining is shown as Mean Fluorescence Intensity (MFI). (G) MutuDCs were pre-incubated with isotype control (-) or blocking anti-DNGR-1 (+). Then, cells were exposed or not to DNGR-1L and further stimulated with WGP. *Tnf*, *Cxcl2* and *Egr2* expression was analyzed by Q-PCR. (H) MutuDCs were exposed to DNGR-1L for the given times. C-type lectin receptors-related regulatory mechanisms such as SHIP-1 phosphorylation and LYN degradation were assessed by immunoblot. (A,B,D-F,H) a representative experiment is shown of at least two performed. (C,G) Mean+SEM of pooled experiments including ≥ 3 individual cultures. Significance was assessed by paired Student's *t*-test between DNGR-1L-treated or not; **p* < 0.05; ***p* < 0.01.

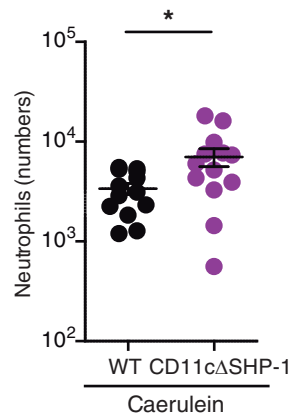


Fig. S9. Increased neutrophil infiltration in pancreas of CD11cΔSHP-1 mice during acute pancreatitis.

Acute pancreatitis was induced by seven intraperitoneal injections of caerulein (50 micrograms/Kg) hourly for 6 hours in *Itgax^{+cre}Ptprn6^{fl/fl}* (CD11cΔSHP-1) and WT littermate mice. Animals were sacrificed 12 hours later and infiltrating neutrophils into the pancreas were monitored by flow cytometry. Mean±SEM of 2 pooled experiments. Each dot represents single mice. Significance was assessed by unpaired Student's *t*-test between genotypes; **p*< 0.05.

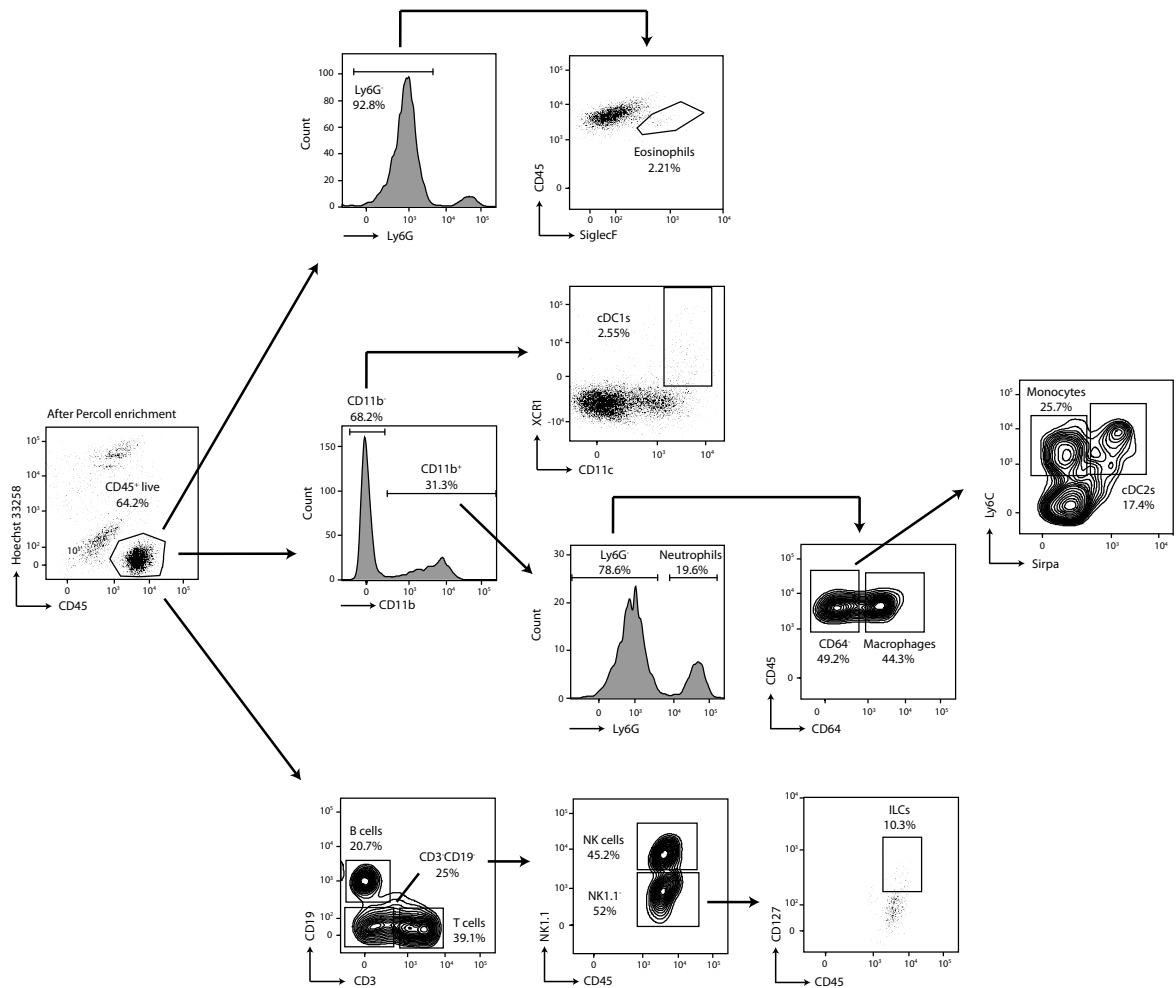


Fig. S10. Gating strategy used to sort infiltrating immune populations from *Candida albicans*-infected kidneys.

Candida albicans was intravenously injected in WT and *Clec9a^{gfp/gfp}* mice. After 2.5 days, kidneys were collected, enriched in CD45⁺ cells by Percoll gradient centrifugation and the illustrated strategy was followed to FACS-sort (from top to bottom) eosinophils, type 1 cDCs (cDC1s), neutrophils, macrophages, monocytes, type 2 DCs (cDC2s), B cells, T cells, natural killer (NK) cells and innate lymphoid cells (ILCs). This gating strategy was used to determine the relative frequency of each population and to isolate each of them for further analysis of Mip-2 expression by qPCR.

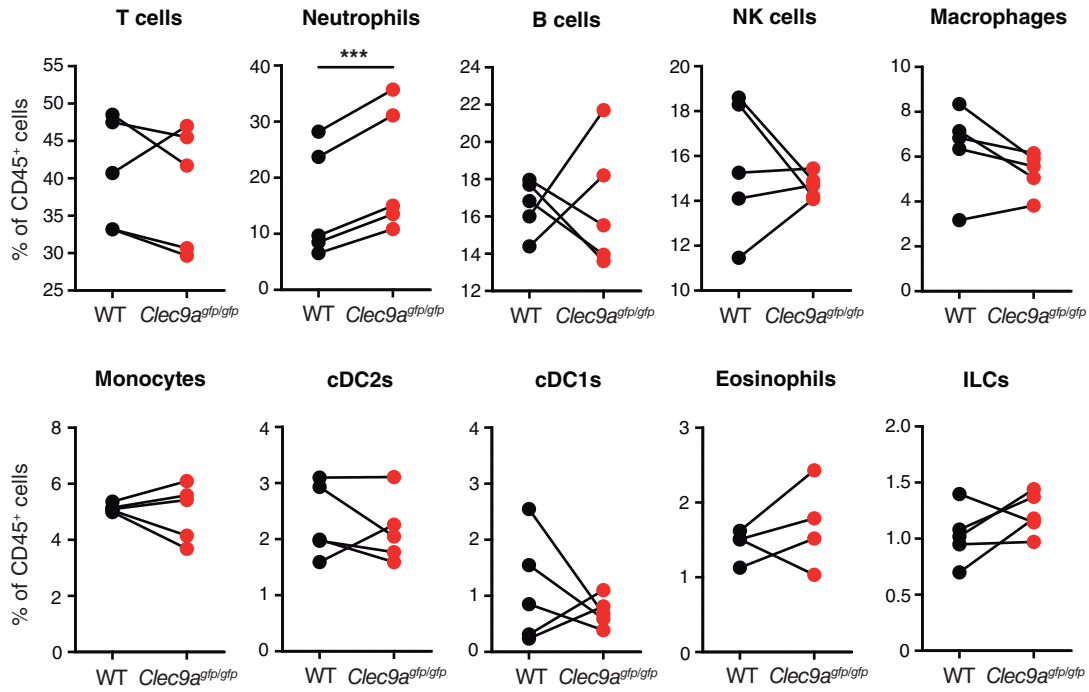


Fig. S11. Among kidney infiltrating CD45⁺ immune cells during systemic candidiasis, only neutrophils are increased in DNGR-1-deficient mice.

Candida albicans was intravenously injected in WT and *Clec9a^{gfp/gfp}* mice. After 2.5 days, kidneys were collected and enriched in CD45⁺ cells by Percoll gradient centrifugation. The frequency of the indicated populations inside the CD45⁺ compartment was analyzed. Paired analysis of 4 or 5 independent experiments represented by dots. Each dot includes a pool of ≥ 4 mice. Significance was assessed by paired Student's *t*-test between genotypes; ****p* < 0.001

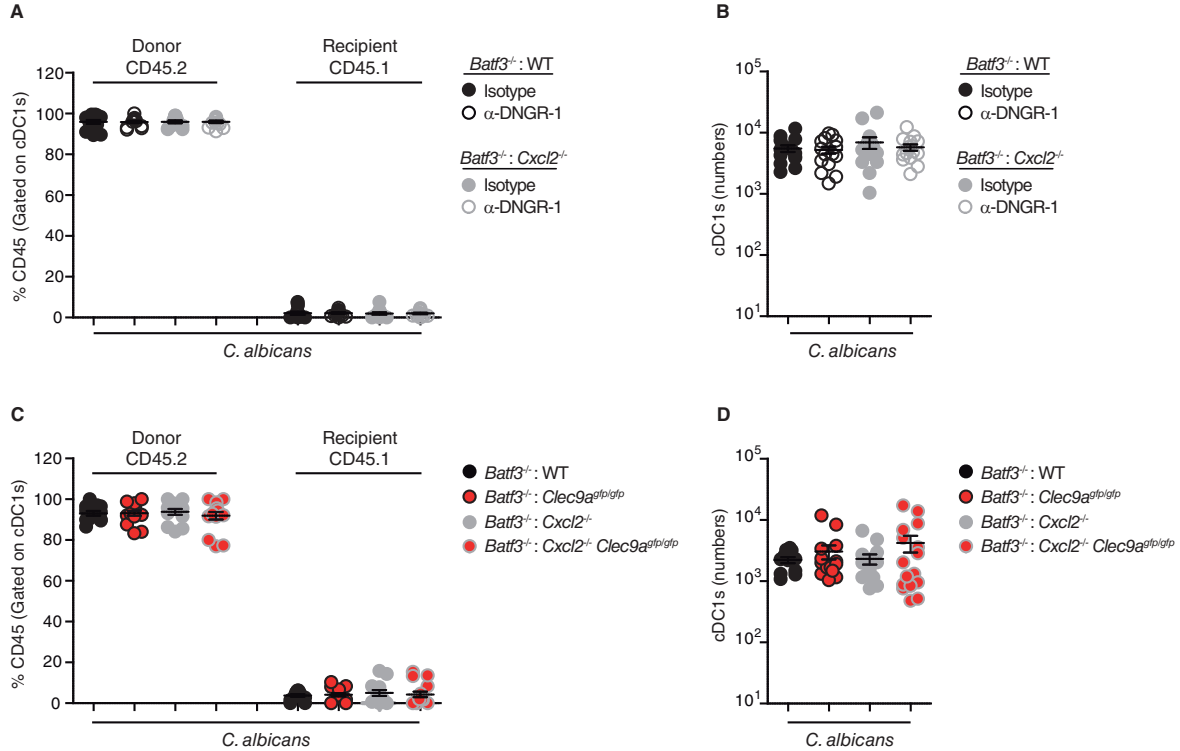


Fig. S12. Reconstitution of mixed bone marrow chimeric mice is not affected by the genotype of the transferred cells.

Mixed bone marrow (BM) chimeric mice were generated as follows. (A, B) Lethally irradiated B6/SJL CD45.1 recipient WT mice were transferred with a mix of 50% of *Batf3^{-/-}* BM cells (CD45.2) and 50% of WT or *Cxcl2^{-/-}* BM cells (CD45.2). Mice were infected with *C. albicans* and anti-DNGR-1 or isotype control antibodies were intraperitoneally injected on day -1 and daily after infection. After 6 days of infection, the expression of the CD45.1 or CD45.2 allotype (A) and the number of renal cDC1s (B) was determined by flow cytometry. (C, D) Alternatively, mixed bone marrow chimeras were generated as described above, consisting of 50% of *Batf3^{-/-}* BM cells and 50% of either WT, *Clec9a^{gfp/gfp}*, *Cxcl2^{-/-}* or *Cxcl2^{-/-}Clec9a^{gfp/gfp}* (CD45.2) BM cells. Mice were infected with *C. albicans* and, after 6 days of infection, the expression of the CD45.1 or CD45.2 allotype (C) and the number of renal cDC1s (D) was determined by flow cytometry. (A-D) Mean \pm SEM of 2 pooled experiments. Each dot represents single mice (n=11-15).

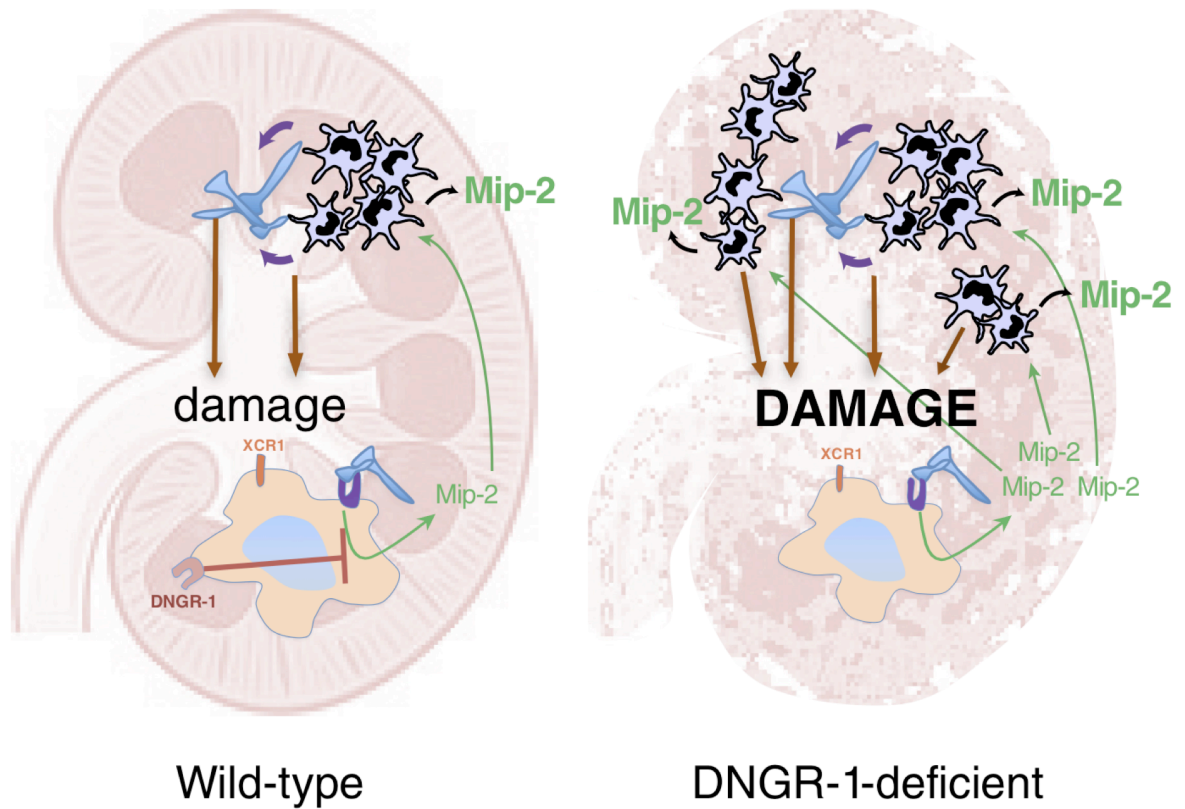


Fig. S13. Working model of the DNGR-1-mediated tissue damage control mechanism under systemic *Candida albicans* infection.

In wild-type mice, sensing of tissue damage by DNGR-1 expressing-cDC1s dampens Mip-2 production by these cells, keeping the infiltration of potentially harmful neutrophils in check. However, in the presence of ongoing tissue damage that is not properly sensed in DNGR-1-deficient mice, the higher production of Mip-2 by cDC1s ignites increased entry of neutrophils that mediate immunopathology.